Robust Control of VO_2-Coated Microbenders Using Self-Sensing Feedback

Emmanuelle Merced, *Student Member, IEEE*, Jun Zhang, *Student Member, IEEE*, Xiaobo Tan, *Senior Member, IEEE*, and Nelson Sepúlveda, *Senior Member, IEEE*

***Abstract*—This paper presents the first studies on robust closed-loop deflection control of vanadium dioxide (VO_2)-based microactuators using self-sensing. The deflection output of the microactuator is estimated by VO_2 resistance-based self-sensing through a high-order polynomial in order to eliminate the need for complicated external sensing mechanisms. An H_∞ robust controller is designed and implemented for precision deflection control, where uncertainties produced by the hysteresis between the deflection and the temperature input and the error in the self-sensing model are accommodated. The performance of the robust controller is tested in experiments under step and multisinusoidal reference inputs and compared to that of a proportional–integral–derivative (PID) controller. The robust controller outperforms the PID controller with 36% and 18% less tracking error for the step and multisinusoidal reference responses, respectively. To further show the robust performance of the H_∞ controller, a multisinusoidal reference tracking experiment with simulated white noise current signal is conducted, where the error using robust control is 34% less than that with PID control.**

***Index Terms*—Microactuators, microelectromechanical systems, robust control, self-sensing feedback, vanadium dioxide (VO_2).**

I. Introduction

In recent years, there has been increased interest in vanadium dioxide (VO_2) for microactuation purposes due to its ability to produce microstructure curvature changes close to or greater than 2000 m^{-1} [1], [2]. A maximum strain energy density of 8.1×10^5 J/m^3 in a temperature window of only 15 °C has been recently reported for a microactuator similar to the one in this paper [3]. The responsible mechanism that drives this behavior is a temperature-dependent solid-to-solid phase transition [4], [5]. The phase-transition in VO_2 is highly hysteretic and comes with drastic changes in crystallographic parameters [6], electrical resistivity [4], and optical transmissivity (mainly for infrared wavelengths) [7]. For a VO_2-coated silicon (Si) cantilever, as the temperature is increased across the transition temperature, which is approximately 68 °C, the VO_2 crystallographic plane parallel to silicon substrate (100) plane contracts abruptly from $(011)_M$ to the $(110)_R$, where M and R denote the monoclinic and rutile VO_2 phases, respectively [1]. This contraction is known to produce strain changes of up to 0.3% in structures of the same geometry used in this paper, which causes the large deflections observed [3]. VO_2 has shown full reversibility after tens of thousands of actuation cycles, showing that the VO_2 stain changes are completely recoverable [8].

For microactuator applications, such as microgripping and micromanipulation, it is vital to measure and control accurately the deflection of the VO_2 device [9]–[12]. Optical measurement methods like laser scattering [1] and interferometry [13] require complicated and large testing setups. While other more compact measurement techniques, like embedded piezoresistors, have been demonstrated [14], [15], they usually involve a relatively complex device fabrication process. Self-sensing, on the other hand, represents an alternative measurement technique, where the variable of interest is estimated by monitoring a coupled parameter—usually much easier to measure and does not need to be embedded in the device—through a mapping model.

Self-sensing has been used effectively in multiple studies as a mechanism for achieving closed-loop control of mechanical displacements in microstructures [16]–[19]. Self-sensing of lead zirconate titanate (PZT) in microactuators has been used to effectively control the vibrations of the device for hard disk drives [17]. By measuring the PZT voltage, which is modeled through a capacitor decoupled in a bridge circuit, the deflection of the PZT-based microactuator can be estimated and controlled [17]. Thermal expansion-based deflection of a microactuator comprising layers of two different materials has also been estimated using the resistance change of one of the materials, based on the monotonic coupled changes in the material resistance and structural deflection as the temperature is varied [18]. A microstructure composed of layers of two different materials was heated, causing both materials to expand at different rates; producing monotonic coupled changes in material's resistance and structure's deflection. Shape memory alloys (SMAs)-based microgrippers have taken advantage of self-sensing by approximating and controlling their strain/deflection using contraction force-to-resistance polynomial models [19]. Although similar to the thermal expansion case, SMAs are highly hysteretic [20], which makes resistance-to-deflection modeling more challenging, thus producing relatively large errors (>5%) between the achieved and desired deflections in tracking-control experiments [21]. These large errors in hysteretic microactuators, like VO_2-based actuators, are undesirable and could be detrimental in applications such as micromanipulation [22], [23], microoptics [24], and microsorting [25], where highly precise control is required.

Manuscript received March 6, 2013; revised July 25, 2013; accepted October 30, 2013. Date of publication November 21, 2013; date of current version May 16, 2014. Recommended by Technical Editor Y. Sun. This work was supported in part by the National Science Foundation under Grant ECCS-1139773, Grant ECCS-0547131, Grant DGE-0802267, and Grant CMMI-1301243.

The authors are with the Department of Electrical and Computer Engineering, Michigan State University, East Lansing, MI 48823 USA (e-mail: mercedem@egr.msu.edu; zhangj78@egr.msu.edu; xbtan@egr.msu.edu; nelsons@egr.msu.edu).

Color versions of one or more of the figures in this paper are available online at http://ieeexplore.ieee.org.

Digital Object Identifier 10.1109/TMECH.2013.2289375

Inverse compensation has been used to reduce the impact of strong hysteresis nonlinearity in smart material actuators [26]–[28]. Although this technique is effective, it is also highly computationally demanding and does not perform robustly against disturbances. Robust control theory has been used in systems based on self-sensing to reduce environmental disturbances and plant uncertainties, although such studies have been typically limited to piezoelectric-based actuators [29]–[32]. The controllers in [29] and [30] were designed to control the deflection of piezoelectric microactuators based on charge measurements. Although external disturbances and model uncertainties were considered for the controller designs, the error between the actual deflection and the reference error was not addressed explicitly. The robust controllers in [31] and [32] were synthesized for suppression of piezoelectric structure vibrations by self-sensing the rate of strain change, where tracking desired reference signals was not a concern. The work done in [31] followed a similar control framework as in [29], although it was designed to follow a desired deflection value of zero (in order to reduce vibrations). Although the controller design in [32] accommodates constraints on control effort, it does not account for effects of model uncertainties, hysteresis, or disturbances. In terms of other hysteretic materials, such as SMAs, there has been no reported work in robust control using self-sensing for deflection control.

This work presents the first study of self-sensing for VO_2 microactuators and its use in closed-loop control of large bending. It is found that the actuator deflection has strong correlation with the resistance in VO_2. Although the resistance change is due to an insulator-to-metal-transition (IMT) and the mechanical change is due to a structural-phase-transition (SPT), these two mechanisms are strongly coupled [33]. Thus, self-sensing is achieved by mapping deflection to resistance and modeling it with a high-order polynomial. By employing this technique, not only the impact of hysteresis can be reduced due to the highly coupled deflection and resistance changes in VO_2, but the measurement setup is also greatly simplified. A robust controller is developed, which takes into account the error in modeling temperature-deflection hysteresis, and environmental disturbances, in order to minimize the tracking error. Unlike previous work on robust bending control of hysteretic microactuators based on self-sensing [29]–[32], the controller in this paper takes into consideration the error between the desired and actual deflection values in order to precisely control the microactuator. The performance of the robust controller is also compared to a proportional-integral-derivative (PID) controller.

II. Experimental Procedures

A. VO_2 Deposition

The VO_2 thin film was deposited, through pulse laser deposition, on a chip containing a Si microcantilever with length, width, and thickness of 300, 35, and 1 μm, respectively. The microactuator chip was attached to a Si test piece and was placed in a vacuum chamber with a mixed gas pressure of argon (40%) and oxygen (60%) at 20 mTorr and maintained through a 30 min deposition. A ceramic heater, controlled at 600 °C, was used to heat the sample during deposition. Although the temperature at the sample was not directly measured, a calibration done before the deposition approximates the temperature at 550 °C. The sample was also rotated throughout the deposition to ensure uniform temperature and thickness distribution. A krypton fluoride excimer laser was focused on a rotating vanadium target 5 cm apart from the sample with an intensity of 350 mJ and a repetition rate of 10 Hz. After deposition, the VO_2 thickness was measured to be 172 nm. To determine the quality of the VO_2, the resistance of the film on top of the test chip was measured as a function of temperature through a heating-cooling cycle (20–85 °C) (*vide infra*). A drop of two orders of magnitude in film resistance is observed, which is similar to resistance changes reported in the literature for stoichiometric polycrystalline VO_2 on Si substrates [15], [16].

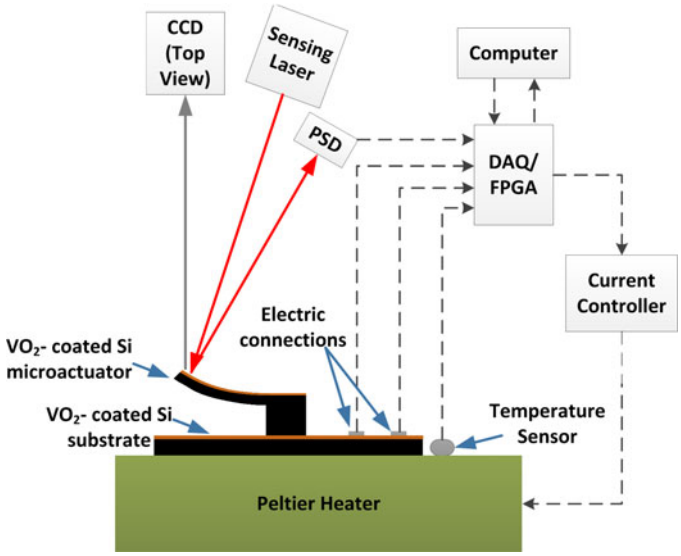

Fig. 1. Schematic for the experimental setup used for deflection and resistance measurements as a function of temperature and the closed-loop control of self-sensed deflection. The microactuator, film, and heater representations are cross-sectional views of the structures.

B. Measurement Setup

The measurement setup shown in Fig. 1 was used for all experiments performed in this paper. The VO_2-coated Si microactuator (shown in cross-sectional view) was attached to the same test piece used during deposition, which was also Si coated with the same VO_2. This test piece was needed in order to create the electrical connections to the VO_2 and measure its resistance. These contacts were located next to the microactuator chip and fabricated by evaporating aluminum through a custom-made metal mask. A voltage divisor (not shown in the schematic) was used in order to measure the resistance of the VO_2 film.

To measure the deflection of the device, a sensing laser ($\lambda = 808$ nm, 0.5 mW) was focused on the tip of the microactuator and the reflected light was then focused on the active area of a position sensitive detector (PSD). A charged-coupled device camera was used to aid in the alignment of the laser. The PSD output was a voltage proportional to the deflection

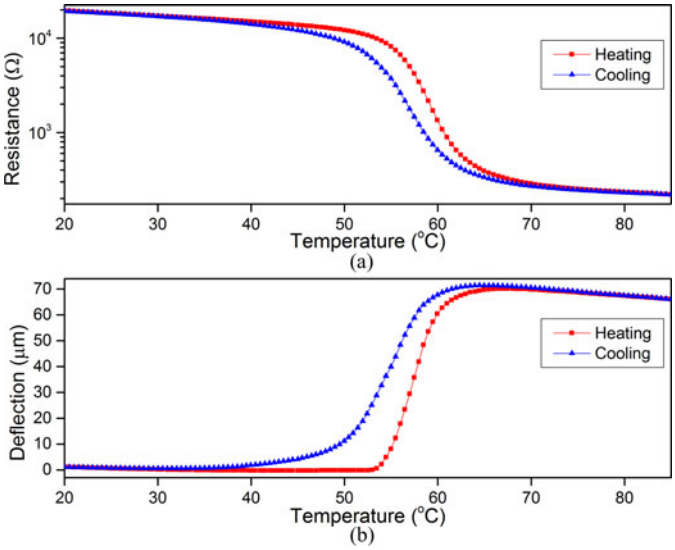

Fig. 2. (a) VO_2 film resistance, and (b) VO_2-coated microactuator actual deflection as a function of temperature through a heating-cooling cycle (20–85 °C). Both variables were simultaneously measured.

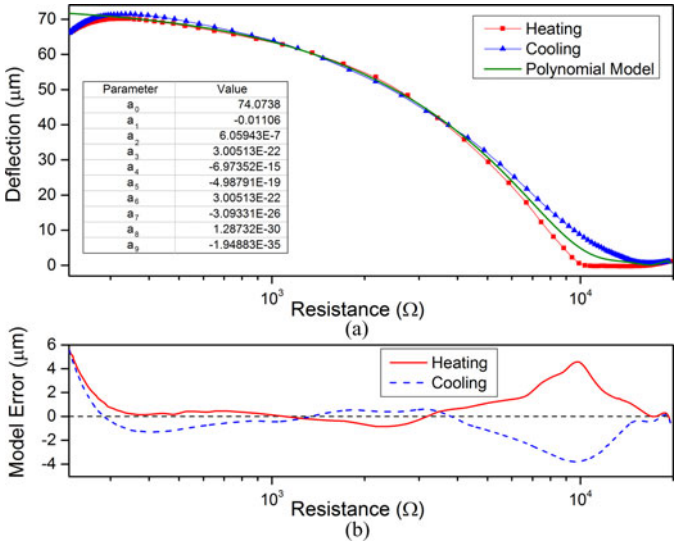

Fig. 3. (a) VO_2-coated microactuator actual deflection as a function of VO_2 film resistance during the heating-cooling cycle. A polynomial function of degree 9 was used to model the deflection-resistance mapping. (b) Maximum model error obtained from the major heating and cooling curves.

of the microactuator, which was calibrated by sideview images of the cantilever at different deflection values. In particular, the calibration of the PSD reading was done by first assigning the initial deflection of the cantilever at 20 °C as 0 μm. Then the sample was heated to 85 °C, which resulted in the maximum deflection of the cantilever, 70 μm, as measured from the side view images of the cantilever. The total voltage change in the PSD output from 20 to 85 °C was 7.8 V, resulting in a measurement sensitivity of 0.111 V/μm. We note that the PSD used in this paper had a resolution of 0.2 μm for the laser spot displacement, while the range for the laser spot displacement was 13.875 mm when the temperature varied from 20 to 85 °C. This means that the PSD reading was highly accurate since the output resolution was 1.4×10^{-5} of the operational range. A Peltier heater was used to control the temperature of the sample. The temperature at the heater was measured with a platinum temperature sensor. A data acquisition card and field programmable gate array (DAQ/FPGA) was used to access the PSD output, the resistance of the VO_2 film, and the temperature sensor output. The DAQ/FPGA system was programmed to either: 1) control the temperature of the Peltier in closed loop in order to measure the deflection of the microactuator and the VO_2 resistance of the test piece simultaneously, or 2) control, using PID or robust controller, the deflection of the microactuator by self-sensing the deflection through resistance. For both cases, the DAQ/FPGA controlled the magnitude of the current signal sent to the Peltier heater. All the variables were controlled and observed in a computer connected with the DAQ/FPGA system.

III. Self-Sensing Deflection

Fig. 2 shows the major heating-cooling cycle of the microactuator deflection and film resistance as a function of temperature. The deflection in this paper is defined as the tip displacement change relative to the initial position. A total deflection of 70 μm and a resistance drop of two orders of magnitude were measured during the VO_2 transition through a temperature span of 15 °C. Both variables were simultaneously measured, and by mapping deflection with resistance, it was observed that the hysteresis between the deflection and the resistance was insignificant, enabling the use of the resistance of the film in the test piece to estimate the deflection without the need of physically measuring its value.

The deflection-resistance mapping is shown in Fig. 3(a), which also includes a ninth-degree polynomial used to estimate the deflection in the experiments. This model was obtained from fitting the average of the heating and cooling curves and was used as the deflection sensing mechanism in the closed-loop deflection control experiments done in this paper. The maximum errors between the heating/cooling curves and the self-sensing model are shown in Fig. 3(b). For a wide range of the resistance, the deflection estimation error was lower than 2 μm whereas slightly larger estimation error was found at the two ends. It is observed that some hysteresis remains. This is believed to be due to the slightly different energy requirements between the IMT and the SPT [33]. This hypothesis is supported by the fact that this difference in energy requirements has been found to be more pronounced at the onset of the phase transition, which would correspond to the higher resistance-low deflection region in Fig. 3(a). Hereinafter, the estimated and measured deflection values will be addressed as self-sensed and actual deflections, respectively.

Two types of controllers will be considered and compared: 1) a PID controller, which only considers the error between the controlled variable (in this case self-sensed deflection) with the desired reference signal, and 2) a robust controller, which aside from considering the error from the controlled variable, also accommodates the error brought by the self-sensing model, noises, and system uncertainties.

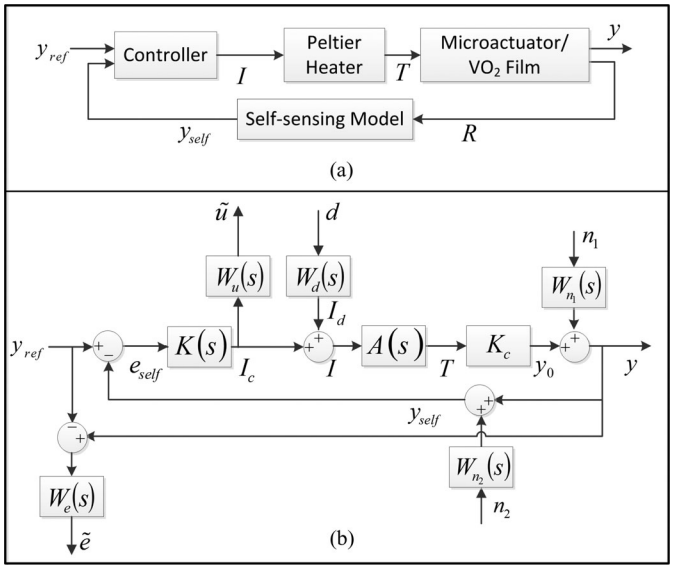

Fig. 4. Block diagrams of the (a) simplified physical closed-loop control system with self-sensing and (b) closed-loop system augmented with weighted functions.

IV. Robust Controller Design

Following H_∞ design techniques [34], an H_∞ controller was designed to accommodate perturbations, noises, and model uncertainties in deflection tracking.

A. Modeling of VO_2 Microactuator

The block diagram for the simplified physical closed-loop system with self-sensing is shown in Fig. 4(a) and the modeled closed-loop system augmented with weighted uncertainties is shown in Fig. 4(b). The variable $y_{\rm ref}$ is defined as the desired deflection output. The input of controller $K(s)$ is the deflection error defined as the difference between $y_{\rm ref}$ and the self-sensed deflection $y_{\rm self}$. The controller output is the current I_c, which is corrupted by I_d that account for environmental disturbances d. $A(s)$ denotes the transfer function for the Peltier heater with temperature T as its output. The hysteresis between temperature T and actual deflection of the VO_2 cantilever y is modeled by the summation of a linear relationship K_c and a noise n_1. The VO_2 film resistance is defined as R. The self-sensing error is taken into consideration through a noise n_2. The functions$W_u, W_d, W_{n_1}, W_{n_2}$, and W_e are weighting functions that represent the importance of the corresponding signals. For example, W_u reflects the control effort constraints and W_e accounts for actual deflection performance. The variables $\tilde{u}$ and $\tilde{e}$ are weighted input and weighted deflection error, respectively.

The temperature dynamics due to the Peltier heater are modeled by a first-order system and a time delay represented by a first-order Padé approximation [35]

$$A(s) = \left(\frac{-\frac{\tau_d}{2}s + 1}{\frac{\tau_d}{2}s + 1}\right)\left(\frac{-A_0}{\tau s + 1}\right) \tag{1}$$

where τ is the time constant associated with the system transient, A_0 is the gain, and τ_d is the time constant associated with the system delay. For the system, in this paper, the deflection transfer function was assumed to have no dynamics since the time constants associated with heat transfer through the cantilever and drag produced by air are much lower than that of the Peltier heater dynamics [8]. Hence, the Peltier heater dynamic response was considered the dominant dynamic in the system under study.

TABLE I
Steady-State Values of Step Experiments for System Identification

Current I (A)	Temperature T (°C)	Time constant τ (s)
−0.2 (heating)	39.7	20.8
−0.4 (cooling)	49.2	27.4
−0.6 (heating)	59.1	22.6
−0.8 (cooling)	70.1	28.2

A series of open-loop step input experiments were conducted to identify the system parameters in (1) and the results are shown in Table I. These were done by manually controlling the current through the Peltier and measuring the temperature transients. The initial current value for each experiment was zero, which corresponded to 25 °C (room temperature). Only heating steps were considered in this parameter identification and a parameter δ was used as an uncertainty parameter due to the differences from heating and cooling with $\delta \in [-1, 1]$. From the measured data, the time constant τ and the gain A_0 of the plant model were calculated to be $25(1 + 0.2\delta)$ and 50 °C/A, respectively. The 0.2 factor that multiplies δ is chosen to cover the range of measured time constants, which span from 20 to 30 s. The time delay τ_d, which is defined here as the time interval between a change in the input current to the system and the temperature response to that signal (dead time), was experimentally measured to be 0.375 s.

There exists a considerable amount of hysteretic nonlinearity between temperature and deflection of the VO_2 microactuator. Although there are several models that capture the hysteresis memory effects in microactuators, such as Preisach [36], [37], Bouc–Wen [27], and Prandtl–Ishlinskii operators [38], due to the complexity consideration in online processing, the hysteresis nonlinearity in this paper was approximated as follows:

$$y = K_c T + n_1 W_{n_1} \tag{2}$$

where K_c is the rate of change in deflection as a function of temperature across the transition, which was identified to be 5.9 μm/°C. The second term in the sum represents the hysteresis modeling error. The self-sensed deflection was then modeled from (2) by

$$y_{\rm self} = K_c T + n_1 W_{n_1} + n_2 W_{n_2} \tag{3}$$

where the third term in the sum represents the self-sensing error obtained with the high-order polynomial in Fig. 3(a). By considering these modeling errors and the remaining weighting functions in Fig. 4(b), a robust control framework can be designed that accommodates environmental disturbances, modeling errors, and uncertainties while effectively controlling the actual deflection of the VO_2-based microactuators.

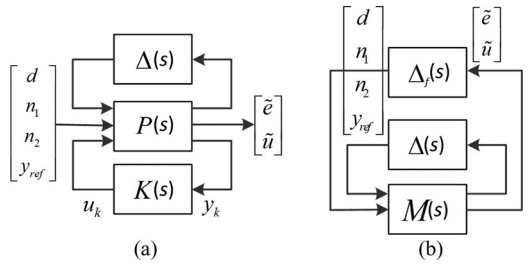

Fig. 5. (a) Framework of H_∞ control for the system and (b) robust performance test by augmenting the uncertainty Δ to M.

B. Robust Control Design

Fig. 5(a) shows the system framework after a linear fractional transformation (LFT), which facilitates the H_∞ controller design process. The transfer functions $\Delta(s), P(s)$, and $K(s)$ denote the uncertainty, interconnection matrix, and controller, respectively. The interconnection matrix is denoted as follows:

$$P(s) = \begin{bmatrix} P_{11}(s) & P_{12}(s) \\ P_{21}(s) & P_{22}(s) \end{bmatrix} \tag{4}$$

where the lower LFT is defined, from (4), as $F_l(P, \Delta_l) = P_{11} + P_{12}\Delta_l (I - P_{22}\Delta_l)^{-1} P_{21}$ and, similarly, the upper LFT as$F_u(P, \Delta_u) = P_{22} + P_{21}\Delta_u (I - P_{11}\Delta_u)^{-1} P_{12}$ with compatible dimensions. The H_∞ control design objective is to find a controller $K(s)$, such that, given $\gamma > 0$, it minimizes the H_∞ norm of the transfer function from the input$w = [d \quad n_1 \quad n_2 \quad y_{\text{ref}}]^T$, which includes the noises, disturbance, and reference signal, to the output $z = [\tilde{e} \quad \tilde{u}]^T$, which includes the control effort and tracking error, by solving

$$\| F_l(F_u(P(s), \mathbf{0}), K(s)) \|_\infty < \gamma \tag{5}$$

where $F_u(P(s),\mathbf{0})$ represents the nominal model and $\| \cdot \|_\infty$ denotes the H_∞ norm.

Choosing appropriate weights is very crucial in robust control design. The main guidelines in this paper are as follows: 1) the control effort weight W_u and disturbance rejection weight W_d are very important across a wide frequency range in order to deal with disturbances with arbitrary frequencies; 2) the actual deflection performance weight W_e is also given importance, especially at low frequencies since the frequency of the desired deflection signal is relatively low due to the relative big time constant of the temperature dynamics; and 3) the noise weightings W_{n_1} and W_{n_2} are more important at higher frequencies since noises will usually have higher frequencies than those of the reference signals. With these guidelines, the transfer functions for the weights are chosen as follows:

$$W_u = 0.12\frac{(s+1)}{\left(\frac{s}{10}+1\right)} \tag{6}$$

$$W_d = 0.1\frac{\left(\frac{s}{2}+1\right)}{(s+1)} \tag{7}$$

$$W_e = 0.09\frac{1}{\left(\frac{s}{10}+1\right)} \tag{8}$$

$$W_{n_1} = 0.002\frac{(s+1)}{\left(\frac{s}{100}+1\right)} \tag{9}$$

$$W_{n_2} = 0.002\frac{(s+1)}{\left(\frac{s}{100}+1\right)}. \tag{10}$$

Based on the model parameters and the weighting functions for the model in Fig. 4(b), the system can be expressed in the following state-space representation, $P(s) = C(sI - A)^{-1} B + D$, where

$$A = \begin{bmatrix} -0.04 & 0 & 0 & 50 & 0 & 0 & -50 \\ 0 & -10 & 0 & 0 & 0 & 0 & 0 \\ -0.24 & 0 & -10 & 0 & 1 & 0 & 0 \\ 0 & 0 & 0 & -5.33 & 0 & 0 & 10.67 \\ 0 & 0 & 0 & 0 & -100 & 0 & 0 \\ 0 & 0 & 0 & 0 & 0 & -100 & 0 \\ 0 & 0 & 0 & 0 & 0 & 0 & -1 \end{bmatrix}$$

$$B = \begin{bmatrix} 0.008 & 0 & 0 & 2.5 & 0 & 50 \\ 0 & 0 & 0 & 0 & 0 & 10.8 \\ 0.048 & -0.2 & 0 & 0 & 1 & 0 \\ 0 & 0 & 0 & -5.33 & 0 & -10.67 \\ 0 & 19.8 & 0 & 0 & 0 & 0 \\ 0 & 0 & 19.8 & 0 & 0 & 0 \\ 0 & 0 & 0 & -0.05 & 0 & 0 \end{bmatrix}$$

$$C = \begin{bmatrix} 1 & 0 & 0 & 0 & 0 & 0 & 0 \\ 0 & 0 & 0.9 & 0 & 0 & 0 & 0 \\ 0 & -1 & 0 & 0 & 0 & 0 & 0 \\ -0.24 & 0 & 0 & 0 & 1 & 1 & 0 \end{bmatrix}$$

$$D = \begin{bmatrix} -0.2 & 0 & 0 & 0 & 0 & 0 \\ 0 & 0 & 0 & 0 & 0 & 0 \\ 0 & 0 & 0 & 0 & 0 & 1.2 \\ 0.048 & -0.2 & -0.2 & 0 & 1 & 0 \end{bmatrix}.$$

Using (5) and the weighting functions from (6) to (10), the transfer function of the controller is calculated based on the algebraic Riccati equation

$$K(s) = \frac{-918(s+1.1)(s+5.3)(s+8.2)(s+100)}{(s+40830)(s+89)(s+1)(s+4.4+/-1.6i)}. \tag{11}$$

In order to implement the resulting controller in (11) it is changed to its discrete z-transform with a sampling time of 125 ms. This sampling time was more than an order of magnitude faster than the closed-loop control response of the system, which ensured a fully reconstructed signal. From (5), the variable γ_{opt} is the optimum over all γ such that the controller is admissible, and, for the controller in (11), it was calculated to be 0.118.

In order to verify the robustness of the closed-loop system, there are two specifications to test: robust stability and robust performance. Black–Nichols diagram has been utilized to

analyze the robust stability in [39], whereas small gain theory [40] and μ synthesis [34], [41] have been utilized to analysis robust stability and robust performance. The latter is a unified approach for analyzing robust stability and robust performance with multiple sources of uncertainties, which is advantageous over the small gain theory approach. Thus, μ synthesis is adopted in this paper, which is represented in Fig. 5(b).

To test for system robust stability, denote

$$M(s) = F_l(P(s), K(s)) = \begin{bmatrix} M_{11}(s) & M_{12}(s) \\ M_{21}(s) & M_{22}(s) \end{bmatrix}. \quad (12)$$

If $||M_{11}||_\infty < 1/\beta$ and $\beta > 0$ are always satisfied for all $\Delta(s)$ with $\| \Delta \|_\infty < \beta$, then the system is robustly stable. For the system shown in Fig. 4(b), using the controller in (11), it is verified with (12) that $||M_{11}||_\infty = 0.26$, which makes the system robustly stable since $\| \Delta \|_\infty = \| \delta \|_\infty < 1$.

To test for robust performance, assume $M(s)$ have$q_1 + q_2$ inputs and $p_1 + p_2$ outputs, $M_{11}(s)$ has q_1 inputs and p_1 outputs, and denote

$$\mathbf{\Delta}_p = \left\{ \begin{bmatrix} \Delta & 0 \\ 0 & \Delta_f \end{bmatrix} : \Delta \in \mathbf{\Delta}, \Delta_f \in \mathbb{C}^{q_2 \times p_2} \right\} \quad (13)$$

where $\mathbf{\Delta} \equiv \delta \in [-1, 1]$ in this paper and Δ_f is shown in Fig. 5(b). A structured singular value can be defined as follows:

$$\mu_{\mathbf{\Delta}_p}(M) = \frac{1}{\min[\bar{\sigma}(\Delta) : \Delta \in \mathbf{\Delta}, \det(I - M\Delta) = 0]} \quad (14)$$

where $\bar{\sigma}(\Delta)$ is the largest singular value of Δ. If for all $\Delta(s)$ with $\| \Delta \|_\infty < \beta$ and $\beta > 0, \sup_{\omega \in \mathbb{R}} \mu_{\mathbf{\Delta}_p}(M(j\omega)) \leq 1/\beta$ is always satisfied, then the system has robust performance. Based on D–K iterations [34], $\sup_{\omega \in R} \mu_{\mathbf{\Delta}_p}(M(j\omega))$ is found to be 0.32, for the case presented here. Hence, the robust performance of the designed robust controller is verified.

V. Results and Discussion

This section provides experimental results using the H_∞ controller derived in the previous section for step and multisinusoidal reference inputs with and without added noise to the current generator. Its performance is compared to that of a proportional-integral-derivative (PID) controller in order to show its robustness to noises and perturbations, as well as the control effort advantages over the PID controller. We have chosen a PID controller instead of a proportional-derivative (PD) controller for the comparison, because, for the dynamics shown in (1), a PD controller would result in nonzero steady-state error for step references even under ideal conditions. The root-mean-square error (RMSE) has been selected to quantify the tracking error in all the experiments, although the average steady-state error has been also calculated for experiments with step reference inputs. Standard deviation (SD) was used to measure the control effort in the multisinusoidal reference input experiment with and without noise.

The parameters of the PID were tuned in simulation based on the same nominal model shown in Fig. 4(b). Since most of the potential applications for the presented microbenders will require high-precision and fast response, the PID controller was designed to have an overshoot of less than 2%, which would ensure accuracy during the transients, and to have a settling time of smaller than 10 s, which would ensure relatively fast response given that the time constant of the Peltier dynamics was approximately 25 s. The resulting controller parameters were: proportional gain $K_p = 0.059$, integral gain $K_i = 0.004$, and derivative gain $K_d = 0.0136$. The obtained transfer function for the controller was transformed to its discrete counterpart in the z-transform with the sampling time of 125 ms for implementation, similar to the robust controller case.

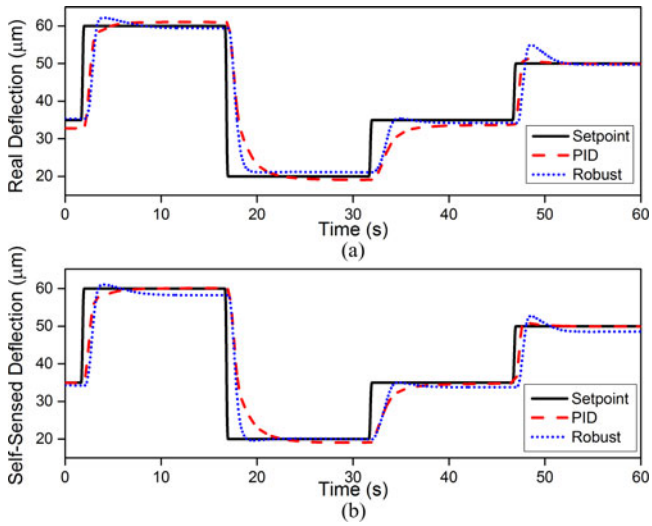

Fig. 6. (a) Actual, and (b) self-sensed microactuator deflection under self-sensed, closed-loop PID and robust control through a series of step reference inputs.

TABLE II
Controller Comparison for Step Reference Tracking

Approach	RMSE (μm)	Average steady-state error (μm)
PID	6.28	1.11
Robust	6.05	0.62

A. Tracking of Step Reference Input

Experiments with step reference inputs were designed so that the microactuator followed a set of three different setpoints, each with duration of 15 s, programmed in the DAQ/FPGA. The goal of these experiments was to study the transient behavior and steady-state error of the robust controller and compare those to the performance of PID controller. Fig. 6(a) and (b) shows the experimental performance in terms of the actual deflection and self-sensed deflection. Although the controlled variable is the self-sensed deflection and a better steady-state performance is observed in Fig. 6(b) for the PID, Fig. 6(a) shows that the actual steady-state deflection under the robust controller is closer to the setpoint for every step value, whereas it has a higher difference under the PID controller. The actual steady-state deflection errors and control efforts are shown in Fig. 7(a) and (b). Table II compares the RMSE of the actual deflection and the average (over three setpoints) steady-state deflection error. Although the largest tracking error for both controllers is similar, the RMSE

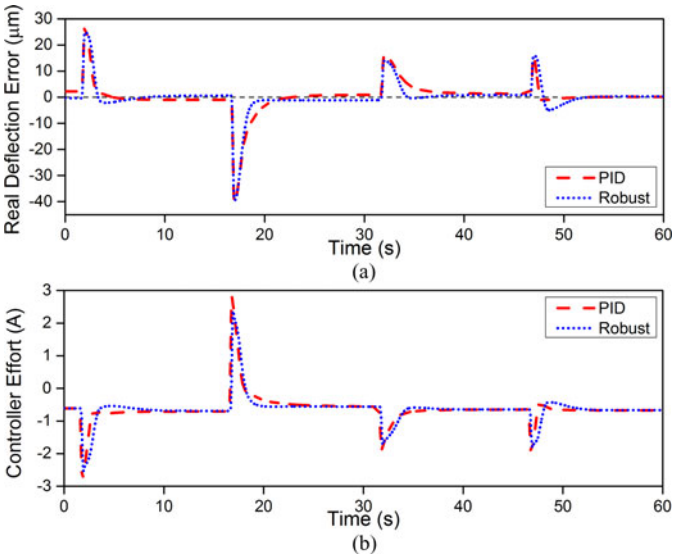

Fig. 7. (a) Actual deflection error and (b) controller effort for the PID and robust control approaches through the step reference tracking experiment.

and average steady-state error under the robust controller are 3.66% and 36%, respectively, less than those of the PID. This proves that the designed robust controller outperforms the PID controller in effectively and robustly reducing the steady-state error of the microactuator's actual deflection by considering the self-sensing modeling error. In practice, the actual deflection performance is of relevance, thus only the actual deflection is provided for the remaining figures in this paper.

The advantages of the robust controller in terms of settling time over the PID controller can be noticed from Fig. 6(a), although there is higher overshoot with the robust controller. A closer examination of the controller efforts, quantified here as the amount of current change, reveals that the robust controller performs slightly higher work than the PID for longer time duration [see Fig. 7(b)], which explains the transient differences.

B. Tracking of Multisinusoidal Reference Input

Experiments involving multisinusoidal reference inputs were carried out to study the performance of the microactuator under continuous input changes. For this experiment, the sum of three different sinusoidal waveforms with frequencies of 0.001, 0.005, and 0.01 Hz, maximum amplitude of 20 μm and an offset of 35μm was chosen as the input signal. The different frequency components of the signal were used to study the deflection control at different frequency values. The amplitude and offset values were chosen in order to cover a wide actuation range throughout the hysteresis. Fig. 8 shows the actual deflection of the microactuator as a function of time with PID and robust control. From the observed data, it is seen that the robust controller performance is better than that of the PID. This is more evident by looking at the tracking errors and control efforts under the two controllers, which are shown in Fig. 9(a) and (b), respectively. The values for RMSE and SD calculated for this experiment are summarized in Table III. From the values in Table III it can be calculated that the robust controller has

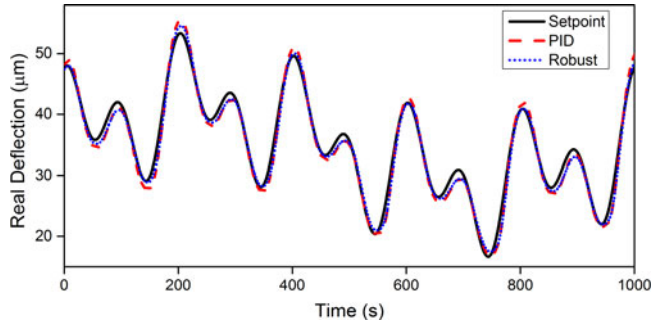

Fig. 8. Microactuator deflection response to a multisinusoidal reference input under PID and robust control.

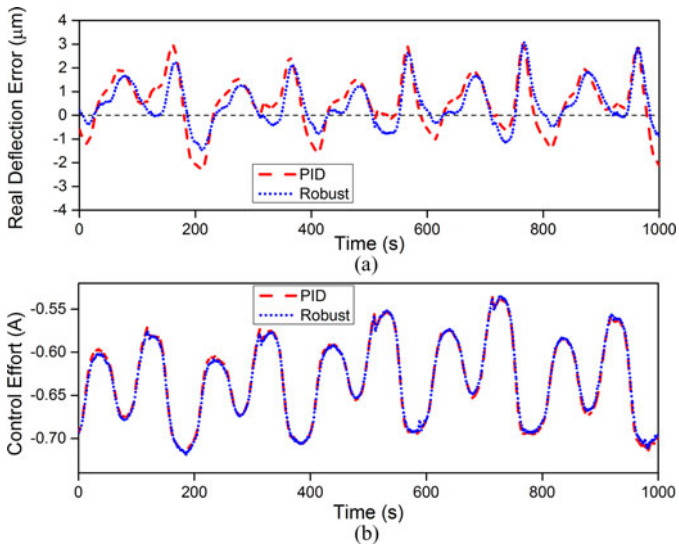

Fig. 9. (a) Actual deflection error and (b) controller effort for the PID and robust control approaches in the multisinusoidal reference tracking experiment.

TABLE III
CONTROLLER COMPARISON FOR MULTISINUSOIDAL REFERENCE TRACKING

Approach	Largest error(μm)	RMSE(μm)	Control effort SD(mA)
PID	3.00	1.24	49.1
Robust	3.07	1.02	48.2

around 18% less tracking RMSE and 1.8% less control effort than the PID controller. The effectiveness of the robust controller in reducing the steady-state error of the actual deflection is again verified experimentally.

C. Noise Rejection for Multisinusoidal Reference Tracking

In order to study the robustness of the H_∞ controller to environmental disturbances, modeled in Fig. 4(b) as I_d, a white noise signal with maximum value of $\pm$ 0.01 A and band-limit of 8 Hz was added to the controller effort. The same input signal used in the multisinusoidal reference input experiment without noise was adopted for this study (see Fig. 8). The white noise amplitude corresponded to 25% of the total current change observed in Fig. 9(b), which represented an overestimate of real-life noise signals due to current variations. Fig. 10(a) shows the actual deflections of the microactuator with the noisy input

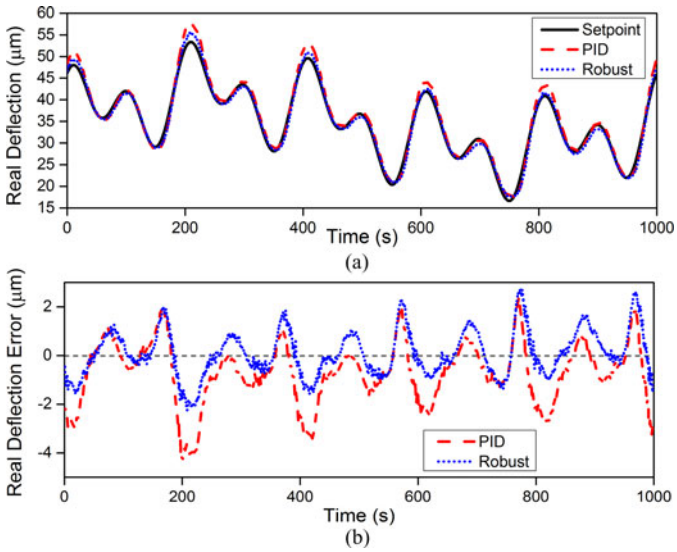

Fig. 10. (a) Microactuator deflection response and (b) error under a multisinusoidal reference input under PID and robust control with induced white noise in current input to the system.

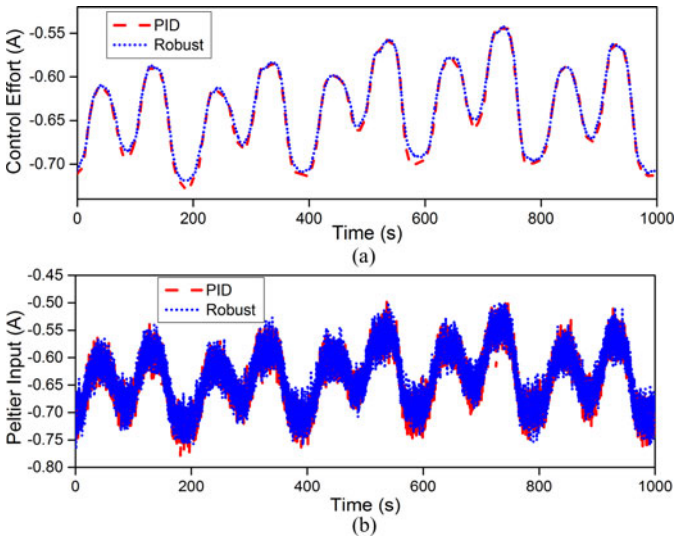

Fig. 11. (a) Control effort and (b) Peltier input for a multisinusoidal reference input under PID and robust closed-control with induced white noise in current input to the system.

under robust and PID control. It is seen from the observed data that the closed-loop deflection system under the H_∞ controller performs robustly against noise disturbances better than with the PID. This difference in performance is evident in Fig. 10(b) where the largest error between actual deflection and reference input with robust control is 3.07 μm and for PID is 4.28 μm. This translates to a 28% decrease in the largest error for the robust controller. While the largest tracking error for PID controller under noisy tracking is 43% larger than the noiseless tracking case, the robust controller ends with not evident deterioration in the largest tracking error. Fig. 11(a) shows the control effort applied by both controllers in these experiments and, for clarity, a separate plot in Fig. 11(b) shows the Peltier input, which includes the controller effort and the white noise. Table IV shows the RMSE and control effort SD values for this

TABLE IV
CONTROLLER COMPARISON FOR MULTISINUSOIDAL REFERENCE TRACKING WITH NOISE

Approach	Largest error(μm)	RMSE(μm)	Control effort SD(mA)
PID	4.28	1.47	33.6
Robust	3.07	0.96	31.6

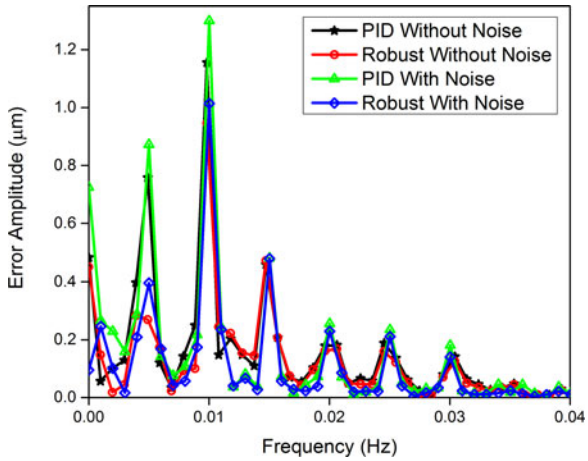

Fig. 12. Frequency spectrum analysis of the tracking errors under the robust controller and the PID controller, for scenarios with and without injected actuation noise.

experiment. For the system with robust control, the RMSE is 34.7% less than with PID, and the control effort SD is 6% less. Although the robust control RMSE in this experiment is close to the one obtained without noise (see Table III), an increase of 18.6% is observed for the system under PID control. This verifies the robust performance and stability of the controller to compensate for deflection control, not only for modeling errors, but also against environmental disturbances.

In addition to the RMSE and the maximum tracking errors, we have further conducted fast Fourier transform of the tracking errors under the PID and H_∞ controllers, for the scenarios with and without injected actuation noises. As shown in Fig. 12, the tracking error under the H_∞ controller is lower than that under the PID controller for all frequency components. This is true for both the cases with and without noise.

VI. CONCLUSION

This paper presented, to the author's best knowledge, the first robust deflection control of a microelectromechanical systems-based VO_2-coated actuator based on self-sensing. The relationship between the resistance and the deflection as a function of temperature of the VO_2 microactuator was provided, and the feasibility of the deflection self-sensing based on resistance was shown and implemented experimentally. A ninth-order polynomial was adopted to model the self-sensing relationship between deflection and resistance. Using the information from the actual deflection and the transfer functions representing the real system, an H_∞ controller was designed and implemented. The effectiveness of the robust controller was compared with a PID controller in terms of tracking accuracy and control effort in a series of experiments. A more accurate model relating the

measured resistance to the deflection, through, for example, a hysteresis operator, could further improve the performance of the proposed controllers at the cost of computational complexity. Investigation of such strategies is the subject of our ongoing work.

ACKNOWLEDGMENT

The authors would like to thank Prof. T. Hogan at Michigan State University for facilitating the pulsed-laser deposition system used for the VO_2 thin films used in this paper.

REFERENCES

[1] A. Rúa, F. E. Fernández, and N. Sepúlveda, "Bending in VO2-coated microcantilevers suitable for thermally activated actuators," *J. Appl. Phys.*, vol. 107, no. 7, Apr. 2010, [Online]. Available: http://scitation.aip.org/content/aip/journal/jap/107/7/10.1063/1.3369282

[2] J. Zhang, E. Merced, N. Sepulveda, and X. Tan, "Modeling and inverse compensation of nonmonotonic hysteresis in VO2-coated microactuators," *IEEE/ASME Trans. Mechatronics*, to be published, DOI: 10.1109/TMECH.2013.2250989, [Online]. Available: http://ieeexplore.ieee.org/stamp/stamp.jsp?tp=&arnumber=6482641

[3] E. Merced, X. Tan, and N. Sepúlveda, "Strain energy density of VO2-based microactuators," *Sens. Actuators A, Phys.*, vol. 196, pp. 30–37, Jul. 2013, [Online]. Available: http://www.sciencedirect.com/science/article/pii/S092442471300126X

[4] F. J. Morin, "Oxides which show a metal-to-insulator transition at the Neel temperature," *Phys. Rev. Lett.*, vol. 3, no. 1, pp. 34–36, Jul. 1959.

[5] G. A. Rozgonyi and D. H. Hensler, "Structural and electrical properties of vanadium dioxide thin films," *J. Vac. Sci. Technol.*, vol. 5, no. 6, pp. 194–199, Nov. 1968.

[6] D. Kucharczyk and T. Niklewski, "Accurate x-ray determination of the lattice-parameters and the thermal-expansion coefficients of VO2 near the transition-temperature," *J. Appl. Crystallogr.*, vol. 12, pp. 370–373, Aug. 1979.

[7] A. S. Barker, Jr., H. W. Verleur, and H. J. Guggenheim, "Infrared optical properties of vanadium dioxide above and below the transition temperature," *Phys. Rev. Lett.*, vol. 17, no. 26, pp. 1286–1289, Dec. 1966.

[8] R. Cabrera, E. Merced, N. Sepúlveda, and F. E. Fernández, "Dynamics of photothermally driven VO2-coated microcantilevers," *J. Appl. Phys.*, vol. 110, no. 9, Nov. 2011, [Online]. Available: http://scitation.aip.org/content/aip/journal/jap/110/9/10.1063/1.3658776

[9] T. C. Duc, G. K. Lau, J. F. Creemer, and P. M. Sarro, "Electrothermal microgripper with large jaw displacement and integrated force sensors," *J. Microelectromech. Syst.*, vol. 17, no. 6, pp. 1546–1555, Dec. 2008.

[10] N. Chronis and L. P. Lee, "Electrothermally activated SU-8 microgripper for single cell manipulation in solution," *J. Microelectromech. Syst.*, vol. 14, no. 4, pp. 857–863, Aug. 2005.

[11] R. Daunton, A. Gallant, D. Wood, and R. Kataky, "A thermally actuated microgripper as an electrochemical sensor with the ability to manipulate single cells," *Chem. Commun.*, vol. 47, no. 22, pp. 6446–6448, Apr. 2011.

[12] C. Gosse and V. Croquette, "Magnetic tweezers: Micromanipulation and force measurement at the molecular level," *Biophys. J.*, vol. 82, no. 6, pp. 3314–3329, Jun. 2002.

[13] C. J. Tay, C. Quan, S. H. Wang, H. M. Shang, and K. C. Chan, "Measurement of a microphone membrane deflection profile using an optical fibre and wedge fringe projection," *Meas. Sci. Technol.*, vol. 12, no. 3, pp. 320–326, Jan. 2001.

[14] T. Ivanov, T. Gotszalk, P. Grabiec, E. Tomerov, and I. W. Rangelow, "Thermally driven micromechanical beam with piezoresistive deflection readout," *Microelectron. Eng.*, vol. 67–68, pp. 550–556, Jun. 2003.

[15] K. Lee, S. S. Lee, J. A. Lee, K. C. Lee, and S. Ji, "Carbon nanotube film piezoresistors embedded in polymer membranes," *Appl. Phys. Lett.*, vol. 96, no. 1, pp. 013511-01–013511-03, Jan. 2010.

[16] J. L. Arlett, J. R. Maloney, B. Gudlewski, M. Muluneh, and M. L. Roukes, "Self-sensing micro- and nanocantilevers with attonewton-scale force resolution," *Nano Lett.*, vol. 6, no. 5, pp. 1000–1006, Apr. 2006.

[17] C. K. Pang, G. X. Guo, B. M. Chen, and T. H. Lee, "Self-sensing actuation for nanopositioning and active-mode damping in dual-stage HDDs," *IEEE/ASME Trans. Mechatronics*, vol. 11, no. 3, pp. 328–338, Jun. 2006.

[18] J. Ouyang and Y. Zhu, "Z-shaped MEMS thermal actuators: Piezoresistive self-sensing and preliminary results for feedback control," *J. Microelectromech. Syst.*, vol. 21, no. 3, pp. 596–604, Jun. 2012.

[19] C. C. Lan, C. M. Lin, and C. H. Fan, "A self-sensing microgripper module with wide handling ranges," *IEEE/ASME Trans. Mechatronics*, vol. 16, no. 1, pp. 141–150, Feb. 2011.

[20] P. Krulevitch, A. P. Lee, P. B. Ramsey, J. C. Trevino, J. Hamilton, and M. A. Northrup, "Thin film shape memory alloy microactuators," *J. Microelectromech. Syst.*, vol. 5, no. 4, pp. 270–282, Dec. 1996.

[21] C. C. Lan and C. H. Fan, "An accurate self-sensing method for the control of shape memory alloy actuated flexures," *Sens. Actuators A, Phys.*, vol. 163, no. 1, pp. 323–332, 2010.

[22] B. D. Chan, F. Mateen, C. L. Chang, K. Icoz, and C. A. Savran, "A compact manually actuated micromanipulator," *J. Microelectromech. Syst.*, vol. 21, no. 1, pp. 7–9, Feb. 2012.

[23] F. Beyeler, A. Neild, S. Oberti, D. J. Bell, Y. Sun, J. Dual, and B. J. Nelson, "Monolithically fabricated microgripper with integrated force sensor for manipulating microobjects and biological cells aligned in an ultrasonic field," *J. Microelectromech. Syst.*, vol. 16, no. 1, pp. 7–15, Feb. 2007.

[24] N. Weber, D. Hertkorn, H. Zappe, and A. Seifert, "Polymer/silicon hard magnetic micromirrors," *J. Microelectromech. Syst.*, vol. 21, no. 5, pp. 1098–1106, Oct. 2012.

[25] G. B. Lee, C. H. Lin, and S. C. Chang, "Micromachine-based multichannel flow cytometers for cell/particle counting and sorting," *J. Micromech. Microeng.*, vol. 15, no. 3, pp. 447–454, Mar. 2005.

[26] S. H. Liu, T. S. Huang, and J. Y. Yen, "Tracking control of shape-memory-alloy actuators based on self-sensing feedback and inverse hysteresis compensation," *Sensors*, vol. 10, no. 1, pp. 112–127, Dec. 2010.

[27] M. Rakotondrabe, "Bouc–Wen modeling and inverse multiplicative structure to compensate hysteresis nonlinearity in piezoelectric actuators," *IEEE Trans. Autom. Sci. Eng.*, vol. 8, no. 2, pp. 428–431, Apr. 2011.

[28] A. Badel, J. Qiu, G. Sebald, and D. Guyomar, "Self-sensing high speed controller for piezoelectric actuator," *J. Intel. Mat. Syst. Str.*, vol. 19, no. 3, pp. 395–405, Mar. 2008.

[29] M. Rakotondrabe, I. A. Ivan, S. Khadraoui, C. Clevy, P. Lutz, and N. Chaillet, "Dynamic displacement self-sensing and robust control of cantilever piezoelectric actuators dedicated for microassembly," in *Proc. IEEE /ASME Int. Conf. Adv. Intell. Mechatronics*, Jul. 6–9, 2010, pp. 557–562.

[30] T. Takigami, K. Oshima, and Y. Hayakawa, "Application of self-sensing actuator to control of a cantilever beam," in *Proc. Amer. Control Conf.*, Jun. 4–6, 1997, pp. 1867–1872.

[31] W. Zhang, J. Qiu, and J. Tani, "Robust vibration control of a plate using self-sensing actuators of piezoelectric patches," *J. Intel. Mat. Syst. Str.*, vol. 15, no. 12, pp. 923–931, Dec. 2004.

[32] U. Boettcher, L. Matthes, B. Knigge, R. A. de Callafon, and F. E. Talke, "Suppression of cross-track vibrations using a self-sensing micro-actuator in hard disk drives," *Microsyst. Technol.*, vol. 18, no. 9–10, pp. 1309–1317, Jun. 2012.

[33] J. Nag, R. F. Haglund, E. A. Payzant, and K. L. More, "Non-congruence of thermally driven structural and electronic transitions in VO_2," *J. Appl. Phys.*, vol. 112, no. 10, Nov. 2012, [Online]. Available: http://scitation.aip.org/content/aip/journal/jap/112/10/10.1063/1.4764040

[34] K. Zhou, *Essentials of Robust Control*. Upper Saddle River, NJ, USA: Prentice-Hall, 1988, pp. 269–299.

[35] Q. C. Zhong, *Robust Control of Time-delay Systems*. London, U.K.: Springer, 2006, pp. 207–208.

[36] X. B. Tan and J. S. Baras, "Modeling and control of hysteresis in magnetostrictive actuators," *Automatica*, vol. 40, no. 9, pp. 1469–1480, Sep. 2004.

[37] B. J. Choi, Y. J. Lee, and B. Y. Choi, "Fast Preisach modeling method for shape memory alloy actuators using major hysteresis loops," *Smart Mater. Struct.*, vol. 13, no. 5, pp. 1069–1080, Aug. 2004.

[38] A. Esbrook, X. Tan, and H. K. Khalil, "Control of systems with hysteresis via servocompensation and its application to nanopositioning," *IEEE Trans. Contr. Syst. Technol.*, vol. 21, no. 3, pp. 725–738, May 2013.

[39] M. Rakotondrabe, Y. Haddab, and P. Lutz, "Quadrilateral modelling and robust control of a nonlinear piezoelectric cantilever," *IEEE Trans. Contr. Syst. Technol.*, vol. 17, no. 3, pp. 528–539, May 2009.

[40] Z. Chen and X. Tan, "A control-oriented and physics-based model for ionic polymer-metal composite actuators," *IEEE/ASME Trans. Mechatronics*, vol. 13, no. 5, pp. 519–529, Oct. 2008.

[41] A. Packard and J. Doyle, "The complex structured singular value," *Automatica*, vol. 29, no. 1, pp. 71–109, Jan. 1993.

Emmanuelle Merced (S'13) received the B.Sc. and M.Sc. degrees in electrical engineering from the University of Puerto Rico, Mayagüez, Puerto Rico, in 2009 and 2011, respectively. He is currently working toward the Ph.D. degree in the Department of Electrical and Computer Engineering, Michigan State University, East Lansing, MI, USA.

He has participated in numerous research and industry-related programs including: memristor group intern at Hewlett–Packard Laboratories, Palo Alto, CA, USA, in 2013, independent contractor at the Universal Technology Corporation, Dayton, OH, USA, in 2011, research intern at the United States Army Corps of Engineers, Vicksburg, MS, USA, in 2009, and research intern at the Power System and Automation Laboratory, Texas A&M University, College Station, TX, USA, in 2008, among others. His research interests include design, fabrication, and implementation of microelectromechanical actuators, smart-materials-based microtransducers, control systems of hysteretic systems, and tunable microresonators.

Prof. Merced was awarded the National Science Foundation Graduate Research Fellowship in 2011 and was named the Electrical Engineering Outstanding Graduate Student for 2012–2013.

Jun Zhang (S'12) received the B.S. degree in automation from the University of Science and Technology of China, Hefei, China, in 2011. He is currently working toward the Ph.D. degree in the Department of Electrical and Computer Engineering, Michigan State University, East Lansing, MI, USA.

His research interests include modeling and control of smart materials.

Prof. Zhang received the Student Best Paper Competition Award at the ASME 2012 Conference on Smart Materials, Adaptive Structures and Intelligent Systems, and the Best Conference Paper in Application Award at the ASME 2013 Dynamic Systems and Control Conference.

Xiaobo Tan (S'97–M'02–SM'11) received the B.Eng. and M.Eng. degrees in automatic control from Tsinghua University, Beijing, China, in 1995 and 1998, respectively, and the Ph.D. degree in electrical and computer engineering from the University of Maryland, College Park, MD, USA, in 2002.

From September 2002 to July 2004, he was a Research Associate with the Institute for Systems Research at the University of Maryland. He joined the faculty of the Department of Electrical and Computer Engineering at Michigan State University (MSU), East Lansing, MI, USA, in 2004, where he is currently an Associate Professor. His current research interests include electroactive polymer sensors and actuators, modeling and control of smart materials, biomimetic robotic fish, mobile sensing in aquatic environments, and collaborative control of autonomous systems.

Dr. Tan is an Associate Editor of *Automatica* and a Technical Editor of the IEEE/ASME TRANSACTIONS ON MECHATRONICS. He served as the Program Chair for the 15th International Conference on Advanced Robotics. He is a recipient of an NSF CAREER Award (2006), MSU Teacher-Scholar Award (2010), and several Best Paper Awards.

Nelson Sepúlveda (S'05–M'06–SM'11) received the B.S. degree in electrical and computer engineering from the University of Puerto Rico, Mayaguez, Puerto Rico, in 2001, and the M.S. and Ph.D. degrees in electrical and computer engineering from Michigan State University (MSU), East Lansing, MI, USA, in 2002 and 2005, respectively.

During the last year of Graduate School, he was with Sandia National Laboratories as part of a fellowship from the Microsystems and Engineering Sciences Applications Program. In January 2006, he joined the Electrical and Computer Engineering faculty, University of Puerto Rico, Mayaguez, Puerto Rico. He was a Visiting Faculty Researcher at the Air Force Research Laboratories in 2006, 2007, and 2013, the National Nanotechnology Infrastructure Network in 2008, and the Cornell Center for Materials Research in 2009, the last two being NSF-funded centers at Cornell University, Ithaca, NY, USA. In 2011, he joined the Department of Electrical and Computer Engineering at MSU, where he is currently an Assistant Professor. His current research interests include smart materials and the integration of such in microelectromechanical systems, with particular emphasis on vanadium dioxide thin films, and the use of the structural phase transition for the development of smart microactuators.

Dr. Sepúlveda received an NSF CAREER Award in 2010.